Self-similar evolution of wave turbulence in Gross-Pitaevskii system

Ying Zhu [1,*] Boris Semisalov [2,3,4] Giorgio Krstulovic [2] and Sergey Nazarenko [1]

[1] *Université Côte d'Azur, CNRS, Institut de Physique de Nice (INPHYNI), 17 rue Julien Lauprêtre 06200 Nice, France*

[2] *Université Côte d'Azur, Observatoire de la Côte d'Azur, CNRS, Laboratoire Lagrange, Boulevard de l'Observatoire CS 34229–F 06304 Nice Cedex 4, France*

[3] *Sobolev Institute of Mathematics SB RAS, 4 Academician Koptyug Avenue, 630090 Novosibirsk, Russia*

[4] *Federal Research Center for Information and Computational Technologies, 6 Academician Lavrentyev Avenue, 630090 Novosibirsk, Russia*

(Received 12 June 2023; accepted 22 November 2023; published 18 December 2023)

We study the universal nonstationary evolution of wave turbulence (WT) in Bose-Einstein condensates (BECs). Their temporal evolution can exhibit different kinds of self-similar behavior corresponding to a large-time asymptotic of the system or to a finite-time blowup. We identify self-similar regimes in BECs by numerically simulating the forced and unforced Gross-Pitaevskii equation (GPE) and the associated wave kinetic equation (WKE) for the direct and inverse cascades, respectively. In both the GPE and the WKE simulations for the direct cascade, we observe the first-kind self-similarity that is fully determined by energy conservation. For the inverse cascade evolution, we verify the existence of a self-similar evolution of the second kind describing self-accelerating dynamics of the spectrum leading to blowup at the zero mode (condensate) at a finite time. We believe that the universal self-similar spectra found in the present paper are as important and relevant for understanding the BEC turbulence in past and future experiments as the commonly studied stationary Kolmogorov-Zakharov (KZ) spectra.

DOI: 10.1103/PhysRevE.108.064207

I. INTRODUCTION

A great number of physical wave systems exhibit states with broadband spectra of excited mutually interacting modes. Such states are called wave turbulence (WT) [1–3], and their examples can be found in classical fluids [4–6], quantum and optical media [7–9], and even in primordial universe [10]. Reference to turbulence in WT occurs because, like in the case of classical hydrodynamics, the WT systems are typically characterized by self-similar cascades of the energy (or another invariant) through scales. Associated with these cascades, there exist stationary self-similar spectra, the so-called Kolmogorov-Zakharov (KZ) spectra, that are analogous to the famous Kolmogorov spectrum of hydrodynamic turbulence, and that are expected in the forced-dissipated WT systems. Search and validation of the KZ spectra, theoretically, numerically, and experimentally, has dominated most of the works on WT [4–6,8,9,11–14]. This interest is explained by the universality of the KZ spectra, i.e., their insensitivity to fine details of forcing and dissipation mechanisms (similar to the universality of the classical Kolmogorov spectrum).

However, temporal evolution leading to the formation of the KZ spectra, as well as the spectrum evolution in unforced systems, can also be universal and exhibit self-similarity. Moreover, such nonstationary solutions are often more relevant in WT realized in laboratories and in natural situations. Self-similar behavior is rather nontrivial and comes in different types corresponding to an infinite-time asymptotic of the system or to a finite-time blowup. Moreover, the same wave system may simultaneously exhibit different kinds of self-similarity in different scale ranges.

In the present paper, we report on a systematical study of nonstationary solutions arising in the forced and unforced Gross-Pitaevskii equation and the associated wave-kinetic equation furnished by the WT theory. In each of the considered settings, we keep our focus on identifying self-similar evolution regimes. Namely, we consider the following representative settings: forced-dissipated direct and inverse cascades and unforced-undissipated (free-decaying) direct and inverse cascades. In the forced-dissipated direct cascade, the energy is injected at low and dissipated at large wave numbers, and in the forced-dissipated inverse cascade, the particles are injected at large and dissipated at low wave numbers. In the unforced-undissipated systems, the direct and inverse cascades arise during a conservative (energy and particle preserving) evolution of spectra toward the high- and low-frequency ranges, respectively. Note that in the unforced-undissipated settings, the solution of the wave-kinetic equation blows up in a finite time t^* marking a nonequilibrium onset of the Bose-Einstein condensation (BEC) into the zero-wave-number mode [15]. Respectively, the WT description fails close to t^* in the low-frequency range due to an accelerated nonlinear (and decelerated linear) dynamics, but the Gross-Pitaevskii evolution continues beyond this time without a blowup. In the forced-dissipated settings, the wave-kinetic blowup can be prevented by introducing dissipation of the zero- and low-frequency modes. In this case, the subsequent evolution leads to the formation of the stationary KZ spectrum [14]. In this paper, we will

*yzhu@unice.fr

aim at systematizing the previous and new findings about the nonstationary evolution of the BEC WT and at presenting a classification of the typical scenarios. Further, we will discuss our results from the point of view of novel perspective designs of the BEC turbulence experiments.

II. THEORETICAL BACKGROUND

A. Gross-Pitaevskii model

Gross-Pitaevskii equation (GPE) describes the evolution of ultra-cold Bosonic gases with repelling interaction potential [16]. For our study, it suffices to work with the dimensionless GPE for the complex wave function $\psi(\mathbf{x}, t)$:

$$\frac{\partial \psi(\mathbf{x}, t)}{\partial t} = i[\nabla^2 - |\psi(\mathbf{x}, t)|^2]\psi(\mathbf{x}, t). \qquad (1)$$

We shall study numerically quasihomogeneous quasi-isotropic turbulence of weakly interacting three-dimensional BEC in a triply periodic cube of side L (and of the volume $V = L^3$). The GPE (1) conserves the total number of particles and energy per unit volume,

$$N = \frac{1}{V}\int_V |\psi(\mathbf{x}, t)|^2\, d\mathbf{x}, \qquad (2a)$$

$$H = \frac{1}{V}\int_V \left[|\nabla\psi(\mathbf{x}, t)|^2 + \frac{1}{2}|\psi(\mathbf{x}, t)|^4\right] d\mathbf{x}, \qquad (2b)$$

respectively.

B. Wave turbulence theory

When the zero-frequency mode (uniform condensate) is negligible, the WT theory for the GPE formulates an asymptotic closure for the waveaction spectrum $n_{\mathbf{k}}(t) \equiv n(\mathbf{k}, t) = \frac{V}{(2\pi)^3}\langle|\hat{\psi}_{\mathbf{k}}(t)|^2\rangle$, where $\hat{\psi}_{\mathbf{k}}(t)$ is the Fourier transform of $\psi(\mathbf{x}, t)$, and the brackets denote averaging over the initial wave statistics. The WT closure is derived under assumptions of small nonlinearity and random initial phases and amplitudes of waves [1,2]. It furnishes a wave-kinetic equation (WKE) with four-wave interactions [7,17]. For an isotropic spectrum, which depends only on the magnitude of the wave vector $k = |\mathbf{k}|$, it is given by

$$\frac{\partial}{\partial t} n_\omega(t) = \frac{4\pi^3}{\sqrt{\omega}} \int \min(\sqrt{\omega}, \sqrt{\omega_1}, \sqrt{\omega_2}, \sqrt{\omega_3})\delta\left(\omega_{23}^{01}\right) \times n_\omega n_1 n_2 n_3 \left(n_\omega^{-1} + n_1^{-1} - n_2^{-1} - n_3^{-1}\right) \times d\omega_1 d\omega_2 d\omega_3, \qquad (3)$$

where ω is the wave frequency determined by the dispersion relation $\omega = k^2$, $n_\omega(t) = n(\omega, t) = n_{\mathbf{k}}(t) = n_k(t)$, $\omega_{23}^{01} \equiv \omega + \omega_1 - \omega_2 - \omega_3$, δ is the Dirac δ function. The integral in (3) is taken over $\omega_1, \omega_2, \omega_3 > 0$.

In this paper, we focus on the spherically integrated wave-action spectrum $n^{\rm rad}(k) = 4\pi k^2 n_\omega$, which is the spectral particle density depending on the wave vector radius k. The WKE for $n_k^{\rm rad} = n^{\rm rad}(k) = n^{\rm rad}(k, t)$ reads

$$\frac{\partial n_k^{\rm rad}}{\partial t} = 2\pi \int \frac{\min(k, k_1, k_2, k_3)}{k\, k_1 k_2 k_3} n_k^{\rm rad} n_{k_1}^{\rm rad} n_{k_2}^{\rm rad} n_{k_3}^{\rm rad} \times \delta\left(\omega_{23}^{01}\right)\left(\frac{k^2}{n_k^{\rm rad}} + \frac{k_1^2}{n_{k_1}^{\rm rad}} - \frac{k_2^2}{n_{k_2}^{\rm rad}} - \frac{k_3^2}{n_{k_3}^{\rm rad}}\right) dk_1 dk_2 dk_3. \qquad (4)$$

WKE conserves the total number of particles and the energy,

$$N = \int_0^\infty n^{\rm rad}(k)\, dk, \qquad (5a)$$

$$E = \int_0^\infty k^2\, n^{\rm rad}(k)\, dk, \qquad (5b)$$

which coincide with Eq. (2a) and with the first term in Eq. (2b) (the second term is small in WT), respectively.

Most central in the WT studies have been the KZ spectra: stationary solutions of the WKE, each realizing a constant spectral flux of an invariant of the system. For the GPE equation, there are two such invariants, N and E and, respectively, there are two KZ spectra. These spectra were proposed in Ref. [7] and discussed in many papers since Refs. [9,11,18,19] but a rigorous systematic derivation of them, including finding the dimensionless pre-factors, was only done recently in Ref. [14]. In that work we obtained and validated numerically, using alongside the GPE and WKE simulations, the following KZ spectra corresponding to the direct energy and the inverse particle cascades—

$$\text{direct}: \quad n^{\rm rad}(k) = 4\pi C_{\rm d} P_0^{1/3} k^{-1} \ln^{-1/3}(k/k_{\rm f}), \quad C_{\rm d} \approx 5.26 \times 10^{-2}, \qquad (6)$$

$$\text{inverse}: \quad n^{\rm rad}(k) = 4\pi C_{\rm i} |Q_0|^{1/3} k^{-1/3}, \quad C_{\rm i} \approx 7.5774045 \times 10^{-2}, \qquad (7)$$

where P_0 and Q_0 are the respective (constant) spectral fluxes of energy and particles through the sphere of radius $k = |\mathbf{k}|$. Note that the log-factor in spectrum (6) is due to the fact that the pure power law $n^{\rm rad}(k) \sim k^{-1}$ ($n_\omega \sim \omega^{-3/2}$) resulting from a dimensional argument corresponds to a marginally divergent integral in the WKE. As a remedy for this situation, the log-correction was suggested on phenomenological grounds in Ref. [7] and proved rigorously in Ref. [14].

The direct and the inverse cascade spectra are different from each other in the following sense. Assuming that the inertial range tends to infinity in the direct cascade spectrum, i.e., that this spectrum extends from the forcing wave number to arbitrarily high k's, the energy integral (5b) is divergent at the upper limit, $k \to \infty$. This corresponds to an infinite energy in physical space, and the respective KZ spectrum is said to have an infinite capacity. However, for the inverse cascade spectrum with an infinite (in the $\log k$ variable) inertial range extending to $k \to 0$ (hence $\log k \to -\infty$), the N-integral in Eq. (5a) is finite (convergent at $k \to 0$). Such a spectrum is said to have a finite capacity, and it corresponds to a finite particle density in the physical space.

Finally, note that because of the $\delta(\omega_{23}^{01})$ term in the WKE (4), if $n_k^{\rm rad} = \text{const}$, then the integral exactly vanishes. This equilibrium (no-flux) spectrum corresponds to thermodynamic energy equipartition and it is known as the

Rayleigh–Jeans spectrum. It represents a special case of more general thermodynamic equilibrium:

$$\text{Rayleigh–Jeans:}\quad n^{\text{rad}}(k) = \frac{4\pi k^2 T}{k^2+\mu}, \tag{8}$$

where T and μ are two (positive) Lagrange multipliers that fix the total energy and mass. They can be interpreted as temperature and chemical potential and play an important role to understand the process of condensation [20–22]. Note that, to make the energy and mass finite, one needs to impose a UV-cutoff $k_{\max}$ in the system. We will come back to this point later.

III. SELF-SIMILAR SOLUTIONS

In Zeldovich's classification, the self-similar solutions can be of two kinds. For the first kind of self-similarity, the self-similar coefficients are fully determined by a conservation law, e.g., energy—like in the spherical shock wave resulting from a point-like energy deposition in an ideal gas. For the second kind of self-similarity, the self-similar coefficients cannot be determined by a conservation law only because most of the respective invariant remains in a volume that is not self-similar—like in the problem of a spherical implosion of a vacuum bubble in gas. Yet, there is also a third kind of self-similarity in which the self-similar coefficients are fixed by a previous evolution stage which is also self-similar [23,24].

In what follows we will see that all three kinds of self-similarity are relevant to the evolving BEC WT. As a general guideline, one should expect the first kind when the respective KZ spectrum has an infinite capacity and the second kind of self-similarity in the finite capacity case. Since in the BEC WT case the direct and inverse cascades have an infinite and finite capacity respectively, they exhibit the first and the second kind self-similarities, respectively. This means, in particular, that the inverse cascade front reaches zero frequency in finite time t^* setting a power law with an anomalous (different from KZ) exponent. This is followed by a reflected-wave spectrum at $t > t^*$ propagating the KZ exponent toward the larger frequencies if dissipation is present at low frequencies. If there is no low-frequency dissipation, then for large values of t one gets the thermodynamic energy equipartition exponent for GPE. In both cases, the reflected wave is described by a self-similar solution of the third kind.

A. The first-kind self-similarity for the direct cascade

Assume that the self-similar solution of Eq. (4) has the following form:

$$n^{\text{rad}}(k,t) = t^{-a} f(\eta) \quad \text{with} \quad \eta = k/t^b. \tag{9}$$

Substituting the above expression into WKE (4), we get

$$\begin{aligned} &-(af(\eta)+b\eta f'(\eta))t^{2a-1}\\ &\quad = 2\pi\int \frac{\min(\eta,\eta_1,\eta_2,\eta_3)}{\eta\,\eta_1\eta_2\eta_3}\\ &\qquad \times\ \delta^{23}_{1\eta^2} f f_1 f_2 f_3\left(\frac{\eta^2}{f}+\frac{\eta_1^2}{f_1}-\frac{\eta_2^2}{f_2}-\frac{\eta_3^2}{f_3}\right) d\eta_1 d\eta_2 d\eta_3, \end{aligned} \tag{10}$$

where $f_i = f(\eta_i)$, $\eta_i = k_i/t^b$ for $i = 1, 2, 3$, $f = f(\eta)$, and $\delta^{23}_{1\eta^2} = \delta(\eta^2+\eta_1^2-\eta_2^2-\eta_3^2)$. The time dependence in the above equation must disappear, which implies $a = 1/2$. Thus, the equation for $f(\eta)$ becomes

$$\begin{aligned} &af(\eta)+b\eta f'(\eta)\\ &\quad = -2\pi\int \frac{\min(\eta,\eta_1,\eta_2,\eta_3)}{\eta\,\eta_1\eta_2\eta_3} f f_1 f_2 f_3\\ &\qquad \times\ \delta^{23}_{1\eta^2}\left(\frac{\eta^2}{f}+\frac{\eta_1^2}{f_1}-\frac{\eta_2^2}{f_2}-\frac{\eta_3^2}{f_3}\right) d\eta_1 d\eta_2 d\eta_3. \end{aligned} \tag{11}$$

Substituting the self-similar form (9) into the definition of energy, we obtain

$$E = t^{3b-a}\int_0^\infty \eta^2 f(\eta)\, d\eta. \tag{12}$$

Consider a temporal evolution of energy obeying the law $E(t) \propto t^\lambda$, with $\lambda = \text{const} \geqslant 0$. Comparing it to Eq. (12), we obtain the scaling exponent $b = 1/6 + \lambda/3$. Therefore, self-similar solution of the first kind is

$$n^{\text{rad}}(k,t)t^{1/2} = f(k/t^b) \text{ with } b = 1/6+\lambda/3. \tag{13}$$

To characterize the temporal propagation of the direct cascade front, let us set a certain value f_c such that $f_c \ll f_{\max}$, where $f_{\max}$ is the maximum value of function $f(\eta)$, find from the equation $f(\eta_{\text{cf}}) = f_c$ the value $\eta_{\text{cf}} = \text{const}$, and define the location of spectral front of the direct cascade at a time moment t as $k_{\text{cf}}(t)$ such that $k_{\text{cf}}(t)/t^b = \eta_{\text{cf}}$.

Far behind the moving front, for $\eta \ll \eta_{\text{cf}}$, we expect a power-law behavior, $f(\eta) \sim \eta^{-x}$ with $x \geqslant 0$. Substituting this power law into (11), we see that in the limit $\eta \to 0$ each term of the left-hand side (LHS) is vanishingly small compared to the right-hand side (RHS) for $x > 0$. Therefore, for $x > 0$ we conclude that for $\eta \ll \eta_{\text{cf}}$ the spectrum tends to the solution of the equation RHS = 0, i.e., to a spectrum whose exponent x is the same as one of the stationary solutions (but not the prefactor!). The borderline case $x = 0$ is similar since it is the energy equipartition case for which LHS = RHS = 0. Thus, at $\eta \ll \eta_{\text{cf}}$, for the forced case we have the direct cascade KZ exponent ($x = 1$), whereas for the unforced case this should be the thermodynamic energy equipartition ($x = 0$). However, the unforced/undissipated case is tricky because the WKE blows up in a finite time t^*, whereas the self-similar solution is usually expected at large times. Nonetheless, we will see that the self-similar solution provides a reasonably good description of the long time evolution of the GPE spectrum (which, in contrast with the solution of WKE, does not blow up).

B. The second-kind self-similarity for the inverse cascade

The inverse cascade has a finite capacity KZ spectrum, and therefore it is expected to exhibit a second-kind self-similarity in its dynamics. This self-similar regime is characterized by the presence of a blowup time t^* and it forms asymptotically very close to this time. Note that the presence of forcing is unessential for this regime due to its self-accelerating blowup nature. Previously, the self-similar solutions of the second kind of the WKE associated with the GPE model were studied in Refs. [15,25–27], and its signatures were seen in the direct numerical simulations of the forced/dissipated 3D GPE in

Ref. [28], and in unforced simulations from Ref. [29], with prior attempts made in Refs. [30,31]. In the present paper, we will recover the previous results and complete them with more detailed considerations of both forced and unforced systems, as well as by considering the setups in which the inverse and the direct cascades show up simultaneously.

For the second-type self-similarity, we assume the following form of the spectrum:

$$n^{\rm rad}(k,t) = g(\xi)\tau^{-r} \text{ with } \xi = k/\tau^m \text{ and } \tau = t^* - t, \quad (14)$$

where t^* is the blowup time. Substituting Eq. (14) into Eq. (4) and requiring that the resulting equation involves only the similarity variable η and not τ, we get $r = 1/2$ and

$$rg(\xi) + m\xi g'(\xi) = 2\pi \int \frac{\min(\xi,\xi_1,\xi_2,\xi_3)}{\xi\,\xi_1\xi_2\xi_3} g g_1 g_2 g_3 \delta^{23}_{1\xi^2} \times \left(\frac{\xi^2}{g} + \frac{\xi_1^2}{g_1} - \frac{\xi_2^2}{g_2} - \frac{\xi_3^2}{g_3}\right) d\xi_1 d\xi_2 d\xi_3, \quad (15)$$

where $g_i = g(\xi_i)$, $\xi_i = k_i/\tau^m$ for $i = 1, 2, 3$, $g = g(\xi)$, and $\delta^{23}_{1\xi^2} = \delta(\xi^2 + \xi_1^2 - \xi_2^2 - \xi_3^2)$. It was shown numerically in Refs. [15,27] and proven analytically in Ref. [26] that $g(\xi) \propto \xi^2$ for $\xi \ll 1$ which corresponds to the thermodynamic energy equipartition spectrum. For $\xi \gg 1$, the spectrum approaches a power law $g(\xi) \propto \xi^{-x^*}$ with exponent $x^* = 1/(2m)$, which is anomalous, i.e., neither KZ nor thermodynamic. This exponent has been numerically explored in several papers by simulating the WKE evolution, seeking for $n_\omega \sim \omega^{-x}$, where $x = 1 + x^*/2$. References [15,25] reported a value of x as 1.24 ($x^* = 0.48$), while in Ref. [27], a value of $x = 1.234$ ($x^* \approx 0.47$) was obtained. More recently, solving directly the nonlinear eigenvalue problem associated with Eq. (15) in Ref. [26], the most carefully determined candidate values were found to be $x = 1.22$ and $x = 1.24$, corresponding to $x^* = 0.44$ and $x^* = 0.48$, respectively.

Note that our self-similar solution of the second kind

$$n^{\rm rad}(k,t)\tau^{1/2} = g(k/\tau^m) \text{ with } m = 1/(2x^*) \quad (16)$$

implies that the spectra $n^{\rm rad}(k,t)$ for various time moments collapse into a single curve $g(\xi)$ when the time is close to t^*. Substituting the established behavior $g(\xi) \propto \xi^2$ as $\xi \to 0$, which was proved in Ref. [26] (based on the nonlocality of interaction of scales $\xi \ll 1$ with scales $\xi \sim 1$), into Eq. (16), we can deduce that the quantity

$$G(\tau) = \lim_{k\to 0} n^{\rm rad}(k,t)\tau^{1/2+2m}/k^2 \quad (17)$$

must tend to a constant as t is approaching t^* from below ($\tau \to +0$). We shall use this as one of the tests of self-similarity in our numerics.

C. The third-kind self-similarity for the inverse cascade

As we explained above, the first- and the second-kind self-similarities are different because in the former case the stationary spectrum is formed right behind the propagating front, whereas for the latter case an anomalous power-law spectrum forms for $t \to t^*$ ($t < t^*$). The anomalous power law is further replaced by a stationary spectrum—the process that takes the form of a reflected wave propagating back from the dissipation wave number to the forcing one. This new type of self-similar behavior was first studied for the direct cascade systems in Refs. [23,24], but it is natural to expect it for all finite-capacity systems, in particular, for the BEC WT inverse cascade considered in the present paper. This behavior does not fit the Zeldovich's first/second-kind classification and, therefore, was named the third-kind self-similarity in Refs. [23,24].

The third-kind self-similarity is realized for $t \to t^*$ ($t > t^*$); it is characterized by the spectrum (14) in which now $\tau = t - t^* > 0$. In the present paper, we will not study such a behavior in detail because the numerical resolution of our simulations is insufficient for making definitive conclusions. However, we will comment on the signatures that are consistent with the reflected wave scenario in the results of the WKE numerics and on the absence of such signatures in the GPE numerics.

D. Free decay: Blowup versus no-blowup initial data

As mentioned in Sec. III B, the second-kind self-similarity is observed for the WKE in the inverse-cascade settings, both with and without forcing. This behavior is a precursor to the condensation at $k = 0$ which sets in at a finite time t^*. Actually, for unforced systems, this kind of evolution is expected only for sufficiently low-k initial data, as follows from the standard Einstein's condensation argument applied to the classical waves [20]. This argument consists in a statement that Bose-Einstein condensation occurs when no equilibrium Rayleigh-Jeans (RJ) spectrum (8) $n^{\rm rad}(k) = 4\pi k^2 T/(k^2 + \mu)$ (with $T, \mu = $ const) can be found containing the same amount of N and E as in the initial condition. (Note that it is necessary to assume that the system is truncated at the UV-cutoff $k_{\rm max}$ to make E and N finite.) Specifically, the minimal possible value of E/N in the RJ spectrum occurs for $\mu = 0$, and this value is equal to $k_{\rm max}^2/3$. Of course, this argument implies that the thermal equilibrium is an attracting state, i.e., that there is a mixing mechanism leading to relaxation to this state either due to a coupling to a thermal bath (not our case) or provided by nonlinear wave interactions (our case). In the latter case, the required mixing may be absent for certain special initial data and the WKE-governed system goes, e.g., through a periodic evolution [32].

The previous discussion implicitly assumes that energy and total number of particles are conserved during the temporal evolution, even in the presence of an UV-cutoff. At first sight, it seems contradictory that a truncated system exhibiting a direct cascade could conserve energy, as one might expect naively that interacting wave modes will excite wave numbers beyond $k_{\rm max}$, creating an energy leakage. However, by truncating a system, one actually kills such interactions so that the cascade can not pass through $k_{\rm max}$.

The introduction of an UV-cutoff in a nonlinear partial differential equation allows for a simple statistical mechanics description of thermal states, as first realized by Lee and Kraichnan for the truncated Euler equation [33,34]. Kraichnan introduced the concept of absolute equilibria in which Fourier modes of the velocity field are in thermal equilibrium and obey Gibbs statistics, i.e., they have the distribution $\propto \exp[-E/T]$, where E is the kinetic energy of the flow.

The relaxation toward thermal equilibrium presents a rich and complex dynamics which exhibits turbulent cascades prior to complete thermalisation [35]. This process was later extended to the cases of helical flows [36], the Burgers equation [37], magnetohydrodynamics [38], and in particular, to the case of the truncated Gross-Pitaevskii equation [21,22]. Note that the RJ spectrum (8) is an absolute equilibrium of the truncated GP system for small amplitude waves. In the context of finite temperature BECs, the truncation of the GP equation is justified by a semi-classical approximation in which only particles with momenta such that $\hbar\omega(k_{\max}) \leqslant k_B T$ are taken into account (with T the temperature and k_B and $\hbar$ the Boltzmann constant and Planck constant). In the context of weakly nonlinear optical waves propagating in a multimode fiber, the frequency cutoff naturally arises from experimental conditions [39]. We introduce in the following the truncated GP and properly define the truncated wave kinetic equation.

1. Truncated Gross-Pitaevskii equation

The truncated GP equation is easily defined from the standard GP equation expressed in Fourier space. It results from a Galerkin projection at the wave number $k_{\max}$ and reads

$$\frac{\partial \hat{\psi}_{\mathbf{k}}}{\partial t} = -ik^2\hat{\psi}_{\mathbf{k}} - \sum_{\mathbf{123}} \theta_k\theta_1\theta_2\theta_3\hat{\psi}^*_{\mathbf{1}}\hat{\psi}_{\mathbf{2}}\hat{\psi}_{\mathbf{3}}\delta^{01}_{23}, \qquad (18)$$

where $\theta_k = 1$, if $|\mathbf{k}| \leqslant k_{\max}$ and $\theta_k = 0$ otherwise. It can be easily seen that this equation derives from the Hamiltonian $H = \sum_{|\mathbf{k}|\leqslant \mathbf{k}_{\max}} k^2|\hat{\psi}_{\mathbf{k}}|^2 + \sum_{\mathbf{1234}} \theta_1\theta_2\theta_3\theta_4\hat{\psi}^*_{\mathbf{1}}\hat{\psi}^*_{\mathbf{2}}\hat{\psi}_{\mathbf{3}}\hat{\psi}_{\mathbf{4}}\delta^{12}_{34}$. The truncated Hamiltonian preserves invariance with respect to the time and phase shifts and, therefore, Eq. (18) also conserves the total energy and the total number of particles.

The truncation of the Gross-Pitaevskii model was first explicitly introduced by Davis *et al.* [40] to study the process of condensation in Bose gases by performing direct numerical simulations of the GP equation. Since then, the truncated (or sometimes called projected) GP equation has become an important model for finite temperature BECs. It has been used for studying the interaction of vortices and particles with thermal waves [41,42], as well as the quantum turbulence at finite temperatures [43]. Note that RJ spectrum (8), and the argument given for classical condensation of waves in Ref. [20] is only qualitative in the case of infinite systems. Indeed, close to the condensation transition, the system becomes fully nonlinear at very low wave numbers and the WT theory can not be applied there. The whole Hamiltonian (2b) should be taken into account, which corresponds to the energy of the well-known $\lambda - \phi^4$ theory, describing second-order phase transitions [21]. However, in finite (e.g., trapped) systems, the lowest wave number is finite, and in principle, the system may remain weakly nonlinear even when all the particles condense at the lowest energy level.

2. Truncated wave kinetic equations

The truncated WKE immediately follows from Eq. (18) and its Hamiltonian, as the truncation can be interpreted as

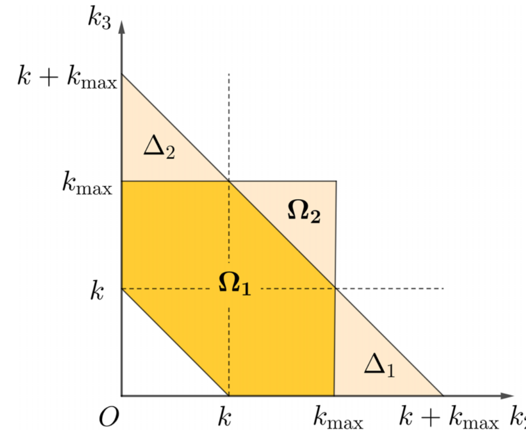

FIG. 1. Domain of integration of the collision term of truncated WKE.

a collisional matrix. It simply reads

$$\frac{\partial n^{\rm rad}_k}{\partial t} = 2\pi \int \theta_k\theta_1\theta_2\theta_3 \frac{\min(k, k_1, k_2, k_3)}{k\, k_1 k_2 k_3} n^{\rm rad}_k n^{\rm rad}_{k_1} n^{\rm rad}_{k_2} n^{\rm rad}_{k_3} \times \delta\big(\omega^{01}_{23}\big)\left(\frac{k^2}{n^{\rm rad}_k} + \frac{k_1^2}{n^{\rm rad}_{k_1}} - \frac{k_2^2}{n^{\rm rad}_{k_2}} - \frac{k_3^2}{n^{\rm rad}_{k_3}}\right) dk_1 dk_2 dk_3, \qquad (19)$$

which also naturally conserves the truncated invariants. The truncation acts on all wave numbers k, k_2, k_3, and $k_1 = k - k_2 - k_3$, which reduces the integration domain to the area Ω_1 in Fig. 1. Note that performing a naive truncation on the WKE, which could be for instance keeping the domains Δ_1, Δ_2, and Ω_2, leads to an energy leak through $k_{\max}$. The spurious consequence of such a choice is discussed in Sec. A.

More interesting, it is well known that the WKE admits an H-theorem which states that the entropy $S = \int \log n_{\mathbf{k}} d\mathbf{k}$ grows monotonically in time [1]. In particular, the theorem holds in the truncated case with the entropy truncated at $k_{\max}$. Moreover, note that the RJ spectra maximize the entropy at fixed total energy and number of particles. Therefore, it is natural to assume that in the absence of finite-time blowup, the truncated WKE solutions will tend to the RJ solution if temperature and chemical potential can be determined.

Having introduced the truncated WKE, we can formulate the following proposition for the freely decaying WKE systems with a UV-cutoff $k_{\max}$. (i) For initial data such that $E/N \geqslant k^2_{\max}/3$, the finite-time blowup at $k = 0$ is absent, and, respectively, no self-similar evolution of the second kind is observed. (ii) Assuming additionally that the initial data is not pathological and there is a suitable mixing present in the system (validity of the H-theorem), the spectrum asymptotes to the RJ spectrum for $t \to \infty$. Conditions for suitable mixing are to be determined. (iii) For initial data with $E/N < k^2_{\max}/3$, the finite-time blowup will occur at $k = 0$ (provided a suitable mixing condition) and, respectively, self-similar evolution of the second kind is observed in the vicinity of the blowup time.

Note that the finite-time blowup for a specific initial condition was rigorously proven in Ref. [32]. In their case, there was no maximum wave number (formally, $k_{\max} = \infty$), so the blowup condition specified above in (iii) was satisfied.

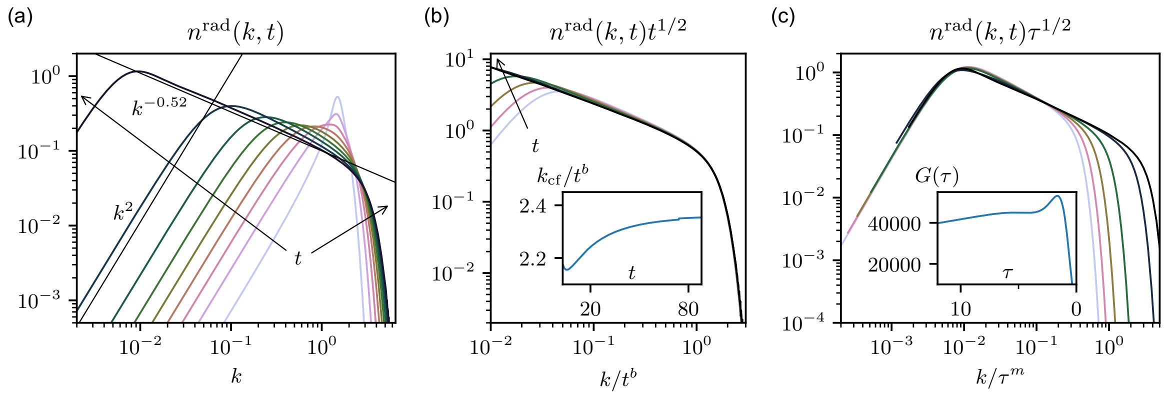

FIG. 2. Numerical results obtained in WKE simulation (case 1) for free-decay case with $k_s = 1.5$: (a) spherically integrated wave-action spectrum $n^{\rm rad}(k,t)$ for the times $t = 10, 20, 30, 40, 50, 60, 70, 80, 88.5$; (b) $n^{\rm rad}(k,t)$ compensated by $t^{1/2}$ vs compensated wave number k/t^b, and inset for the time evolution of the compensated wave front $k_{\rm cf}/t^b$; (c) $n^{\rm rad}(k,t)$ compensated by $\tau^{1/2}$ vs compensated wave number k/τ^m, and inset for $G(\tau)$ for the time close to blowing up. Spectra in panels (b) and (c) are given for $t = 80, 82, 84, 86, 88, 88.5$.

For the forced systems, there will be a continuous supply of particles, and we can conjecture that the WKE system will always blow up in a finite time (in the absence of dissipation at the low-k region) irrespective of the initial condition and the forcing strength.

IV. NUMERICAL RESULTS

A. Numerical setup

To study the self-similar behavior of the different kinds, we consider two types of setups: the unforced (free-decay) and the forced systems. We further subdivide the forced setups into the direct and the inverse cascades—with forcing at low and at high wave numbers, respectively. Moreover, we consider the inverse cascade in two cases exhibiting qualitatively different behaviors—with and without dissipation at the smallest wave numbers. The latter case leads to condensation.

We numerically simulate GPE (1) and WKE (3). The GPE is solved by using the standard massively parallel pseudospectral code FROST [44] with a fourth-order exponential Runge-Kutta temporal scheme (see Ref. [29]). We discretize the L^3-periodic box using N_p^3 collocation points. The WKE is solved using the code developed in Refs. [14,26,29]. This code uses a decomposition of the integration domain in the RHS of Eq. (3), so that in each subdomain the integrand is a highly smooth function. We simulate the WKE in the interval $\omega \in [\omega_{\min}, \omega_{\max}]$, and we set $n_\omega = n_{\omega_{\min}}$ for $\omega < \omega_{\min}$, and $n_\omega = 0$ for $\omega > \omega_{\max}$. The second-order Runge-Kutta scheme is employed to march the time for free-decay cases, and a new approach inspired by Chebyshev interpolation and schemes described in Ref. [45] is used for the time integration in the forced cases. The WKE solvers employed in Refs. [14,29] attained superior resolution and broader computing ranges while demanding significantly fewer computing resources than the GPE solver.

For GPE simulations, the spherically integrated wave-action spectrum is computed as

$$n^{\rm rad}(k,t) = \frac{1}{D_k}\sum_{\mathbf{k}\in\Gamma_k} |\hat{\psi}(\mathbf{k},t)|^2, \tag{20}$$

where Γ_k is the spherical shell around $|\mathbf{k}| = k$ with thickness D_k. In WKE simulations, $n^{\rm rad}(k,t) = 4\pi\omega n_\omega(t)$.

In all direct-cascade simulations, the propagation of the spectral front $k_{\rm cf}(t)$ is measured by setting a small threshold value ε and finding for different t the value $k_{\rm cf}$ such that $n^{\rm rad}(k_{\rm cf},t) = \varepsilon$.

B. Free-decay simulations for low E/N

For the free-decay setup, we will, first of all, consider cases which (according to our conjecture in Sec. III D) satisfy the finite-time blowup condition for WKE, $E/N < k_{\max}^2/3$. We start simulations of these cases with Gaussian-shaped spectra, similar to the ones used in Ref. [29]:

$$n^{\rm rad}(k,0) = g_0 \exp\left(\frac{-(k-k_s)^2}{\sigma^2}\right). \tag{21}$$

We present three free-decay simulations (case 1, case 3, and case 4) with the parameters shown in Table I. Figure 2 is obtained by performing WKE simulation using the parameters of case 1 described in Table I. The initial spectrum was centered at $k_s = 1.5$. We took essential care of setting the distribution of the k-grid points to guarantee high accuracy at both small and large k's. Figure 2(a) shows the dual cascade of wave-action $n^{\rm rad}(k,t)$ for the values of time $t \in [10, 88.5]$. The front of $n^{\rm rad}(k,t)$ propagating to the left develops a thermal particle-equipartition scaling $\sim k^2$, as was also discussed in Refs. [26,29]. At $t = 88.5$—close to the blowup time $t^* \approx 89.5$—the scaling $\sim k^{-0.52}$ is seen between the front

TABLE I. Numerical parameters for the free-decay simulations.

Case	Model	$\omega_{\min}$	$\omega_{\max}$	k_s	g_0	σ
1	WKE	10^{-5}	10	1.5	1	0.2
2	WKE	10^{-2}	86	55	1	2.5
Case	Model	L	N_p	k_s	g_0	σ
3	GPE	8π	720	1.5	1	0.2
4	GPE	8π	512	22	1	2.5
5	GPE	8π	512	35	2	1

propagating to the left and the initial peak. For late preblowup times $t \in [80, 88.5]$, in Fig. 2(b) we plot self-similar solutions of the first kind given by Eq. (13) with $\lambda = 0$, $b = 1/6$ (corresponding to the free-decay case), i.e., we plot $n^{\mathrm{rad}}(k,t)t^{1/2}$ versus $k/t^{1/6}$. Respectively, for the same period of time, in Fig. 2(c) we show a self-similar solution of the second kind given by Eq. (16) with $x^* = 0.52$ and $t^* = 89.5$ (i.e., $n^{\mathrm{rad}}(k,t)\tau^{1/2}$ versus $k/\tau^{1/1.04}$). Inset in Fig. 2(b) presents the time evolution of the compensated spectral wave-action front k_{cf}/t^b in the direct cascade setting. The fact that k_{cf}/t^b tends to be a constant at late times is in almost perfect agreement with the prediction of first-kind self-similarity with $b = 1/6$. However, Fig. 2(c) shows a perfect collapse of plots $n^{\mathrm{rad}}(k,t)\tau^{1/2}$ versus k/τ^m onto the same curve in the inverse cascade setting. Moreover, in the interval $2 < \tau < 7$ we obtain almost constant $G(\tau)$ as predicted by Eq. (17) for small τ, see the inset of Fig. 2(c). This dependence breaks down for very small τ because of the presence of the minimal frequency $\omega_{\min}$ and a small uncertainty in finding t^* in numerics.

It is remarkable that we can see self-similarities of both the first and the second kinds in one single WKE simulation. This is mostly because of the efficient numerical method that allows adaptive k- (or ω-)space discretization with great accuracy. However, the blowup phenomenon in WKE evolution means that one cannot continue the WKE solution beyond $t = t^*$, whereas formally the self-similar solution of the first-kind (13) is expected asymptotically as $t \to \infty$. Taking into account that the direct cascade propagation in the free-decay situation is quite slow ($k_{\mathrm{cf}} \sim t^{1/6}$), it is worth noting that one can observe only the tendency of k_{cf}/t^b to a constant, see the inset of Fig. 2(b). Even though, it is surprising to see that the self-similar behavior in Fig. 2(b) develops relatively early in time.

Simulating GPE is more challenging than WKE, and presently it is impossible to include a sufficiently wide range of scales for observing self-similarities of both the first and the second kind simultaneously in one numerical run. Thus, we ran two different setups with the initial spectrum in the low and high k's to observe the first- and the second-kind self-similarities in the direct and the inverse cascades, separately. To implement a direct cascade for the free-decay case, we simulate GPE (case 3 in Table I) using the same initial $n^{\mathrm{rad}}(k,0)$ as in case 1. However, the GPE discretization is much coarser than the one used for WKE, so the initial data is in the k's where the discreteness is substantial (with the maximum at the wave number equal to the six wave number spacings $2\pi/L$). For this precise reason the inverse cascade evolution is suppressed from the beginning, and the direct cascade dynamics can be viewed as post-t^*. Note that we add friction $D_{\mathbf{0}} = 10^3$ at $k = 0$ (see Sec. IV D for the definition of $D_{\mathbf{0}}$) to effectively prevent the condensation. It should be emphasized that D_0 needs to be sufficiently large, typically $D_0 \geqslant 10^3$ to guarantee the condensate rate $n^{\mathrm{rad}}(0,t)/N < 10^{-4}$ across all relevant simulations. After a small initial change ($\sim$0.1% for $0 < t < 150$) the relative deviations of the particle and energy densities N and H remain constant with accuracy $\sim$0.01%, which means that the choice $\lambda = 0$ in (13) is still suitable. We present the time evolution of wave-action spectra and the self-similar functions of first-kind obtained in this simulation in Figs. 3(a) and 3(b),

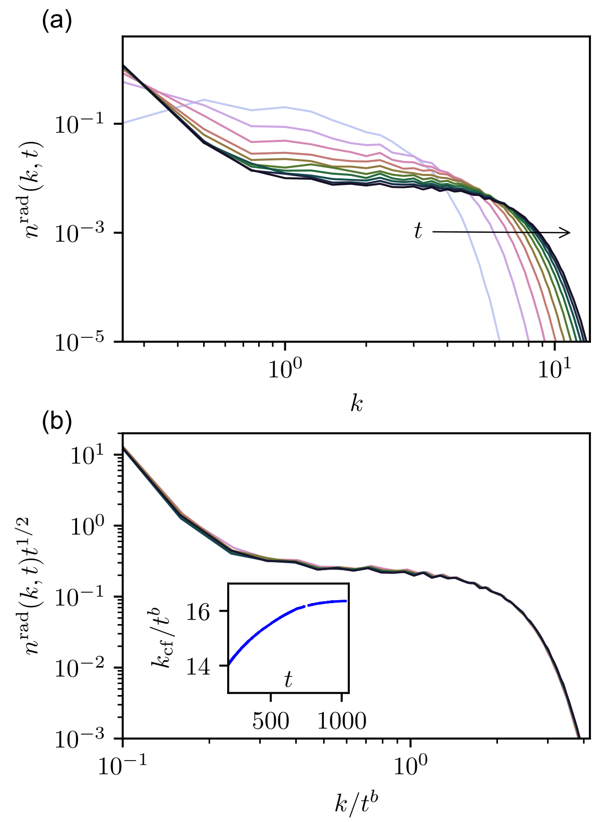

FIG. 3. Numerical results for free-decay GPE simulation (case 3) with $k_s = 1.5$. (a) spherically integrated wave-action spectrum $n^{\mathrm{rad}}(k,t)$ for times $t = 100, 200, 300, 400, 500, 600, 700, 800, 900, 1000$; (b) $n^{\mathrm{rad}}(k,t)$ compensated by $t^{1/2}$ vs compensated wave number k/t^b for times $t = 850, 880, 910, 940, 970, 1000$ and inset for the time evolution of the compensated wavefront k_{cf}/t^b.

respectively, and in the inset of the Fig. 3(b)—time evolution of the compensated spectral front for the direct cascade. At late times, thermal-like equilibrium energy equipartition scaling $\sim k^0$ is observed at the intermediate k-range (between the low-k condensate and the high-k spectral front) as predicted. Also as predicted by the first-kind self-similarity, we observe the collapse of curves $n^{\mathrm{rad}}(k,t)t^{1/2}$ versus k/t^b for different t's, and we see an asymptotic tendency of k_{cf}/t^b to a constant. It is noteworthy that the recent experiment [46] achieved dual cascades with almost constant N and H, reporting a value of $b \approx 0.14$. This finding closely aligns to our prediction $b = 1/6$. Note that even though the GPE and the WKE runs (cases 3 and 1, respectively) share the same initial spectrum, the results obtained by these two simulations deviate quickly because of totally different discretization in k-space. The GPE simulation bypasses the pre-t^* evolution, whereas the WKE evolution ends at t^*. In principle, one could regularise the WKE for describing the post-t^* evolution by coupling it to an equation for the condensate mode $k = 0$, as it is done in Refs. [15,25], but studying the resulting equation is beyond the scope of the present paper. It is interesting, however, that the energy equipartition spectrum observed in our GPE simulation was also claimed to be relevant to the post-t^* evolution of the regularized WKE-condensate system in Refs. [15,25]. The second kind of self-similarity is

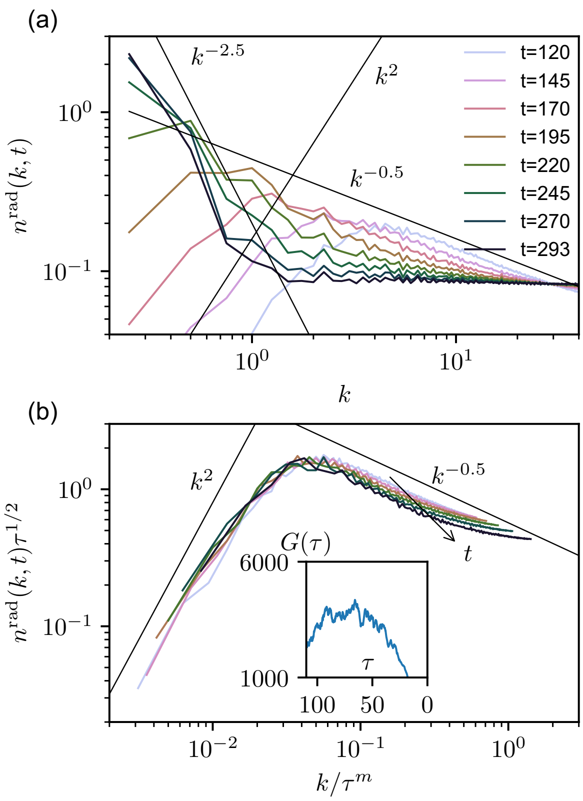

FIG. 4. Numerical results for free-decay GPE simulation (case 4) with $k_s = 22$: (a) evolution of the spherically integrated wave-action spectrum $n^{\rm rad}(k,t)$; (b) the spectrum $n^{\rm rad}(k,t)$ compensated by $\tau^{1/2}$ vs compensated wave number k/τ^m for $t =$ 120, 130, 140, 150, 160, 170. Inset: $G(\tau)$ for the time close to the blowup.

also studied via GPE free-decay simulations with an initial spectrum centered at relatively large wave number $k_s = 22$ (which is yet low enough for the WKE blowup condition, $E/N < k_{\rm max}^2/3$); see case 4 in Table I. Figure 4(a) presents the late time evolution of $n^{\rm rad}(k,t)$ for $t \in [120, 293]$ (early time behavior was discussed in Ref. [29]). One can see clearly the second kind self-similarity for $t \in [120, 170]$ with k^2-scaling at low k's and $k^{-0.5}$-scaling at large k's. The shape of $n^{\rm rad}(k,t)$ starts to change after $t = 170$ showing rapid accumulation of waves in the smallest k (condensation). We observe and quasithermal (energy-equipartition) constant spectra at high k's. Similar behavior was reported in Ref. [28] for the GPE simulations with forcing at large k's. This confirms that the forcing is not important for the self-similarity of the second kind because the characteristic time associated with the forcing is much greater than the characteristic nonlinear time near t^*. We estimate the dependencies of $n^{\rm rad}(k,t)\tau^{1/2}$ on k/τ^m with $x^* =$ 0.5 by using Eq. (16) for each value of t^* in a finely girded range of (170, 230]. This investigation focuses on the data within the established self-similar regime. The value $t^* \approx 200$ minimizes the least-square deviations of the data during the intermediate self-similar phase ($t \in [120, 170]$). Figure 4(b) plots the self-similar functions $n^{\rm rad}(k,t)\tau^{1/2}$ versus k/τ^m for $t \in [120, 170]$. A visible collapse of curves is observed except for high k. We also find a relatively constant $G(\tau)$ for $30 \leqslant \tau \leqslant 100$ in the inset, which coincides with the self-similarity for $t \in [120, 170]$. Note that, unlike WKE, the GPE evolution does not lead to a blowup, and the self-similarity of the second kind is observed as an approximate intermediate asymptotic only. This is natural because the WKE fails to be applicable while approaching t^* both because of the rapid nonlinearity growth and the increased sharpness of the spectrum at low k's where the discreteness of the k-space is essential. This results in the long-term deceleration of GPE dynamics compared to WKE. For the GPE we should also note that the condensate does not occur at the mode $k = 0$ only, like in WKE, but takes a form of a sharp spectrum at low k's. We suggest a scaling of $\sim k^{-2.5}$ as a visual guide, obtained by fitting the data on a limited number of grid points, but this scaling is probably not universal.

C. Free-decay simulations for high E/N

Now, let us consider cases which (according to our conjecture in Sec. III D) satisfy the no-blowup condition for WKE, $E/N \geqslant k_{\rm max}^2/3$. We take initial conditions as case 2 in Table I for WKE simulation, and as case 5 for GPE simulation, respectively. The simulation results are presented in Fig. 5. The time evolution of spectra $n^{\rm rad}(k,t)$ obtained by solving GPE are given in panel (a) for $t \in [0, 320]$, and the results obtained by solving WKE are given in panel (b) for $t \in [0, 2000]$. For GPE simulation, as predicted in Sec. III D, we see neither a tendency to low-k condensation nor any signatures inherent to self-similar behavior of the second kind. The spectrum quickly takes form $n^{\rm rad}(k,t) = A(t)\,k^2$ in a widening k range, with $A(t) \to$ const for $t \to \infty$, as shown in Fig. 5(c) [t_c is defined as the time such that $A(t_c)$ has 1% deviation from $A(\infty)$]. In other words, the spectrum asymptotes to the (stationary) RJ spectrum with $\mu/T \to \infty$ which is a thermodynamic state describing the particle equipartition. Note that the particle equipartition is realized instead of any other spectrum in the RJ family because it corresponds to the chosen initial condition with E/N close to its maximum possible value $k_{\rm max}^2$. Similarly, the truncated WKE evolution in Figs. 5(b) and 5(c) also exhibits the same behavior as the GPE with a clear thermalization to the RJ spectrum.

The case with a naive truncation in which energy leaks through the cutoff $k_{\rm max}$ is discussed in the Appendix. In short, this leakage leads to a decreasing value of E/N, such that even if initially it is larger than $k_{\rm max}^2/3$, after some time this condition is violated followed by a condensation-type blowup in finite time.

D. Simulations with forcing

Unlike the free-decay case, all the simulations with forcing start with a zero initial field. In GPE simulations, we add the forcing term $F_{\bf k}(t)$ and the dissipation term $-D_{\bf k}\widehat{\psi}_{\bf k}(t)$ to the Fourier transform of the RHS of GPE (1). In the GPE simulation for the direct cascade (case 6 in Table II, we add forcing by fixing $n^{\rm rad}(k,t) = n_{\rm f}$ on a spherical shell in k-space with $0.5 \leqslant k \leqslant k_{\rm f}$, whereas for the inverse cascade (cases 6 and 7 in Table II), for a narrow spherical shell $k_{\rm f} - 1 = 124 \leqslant k \leqslant k_{\rm f} + 1 = 126$ we add forcing terms obeying the Brownian motion $dF_{\bf k}(t) = f_0 dW_{\bf k}$, where $W_{\bf k}$ is the Wiener process and

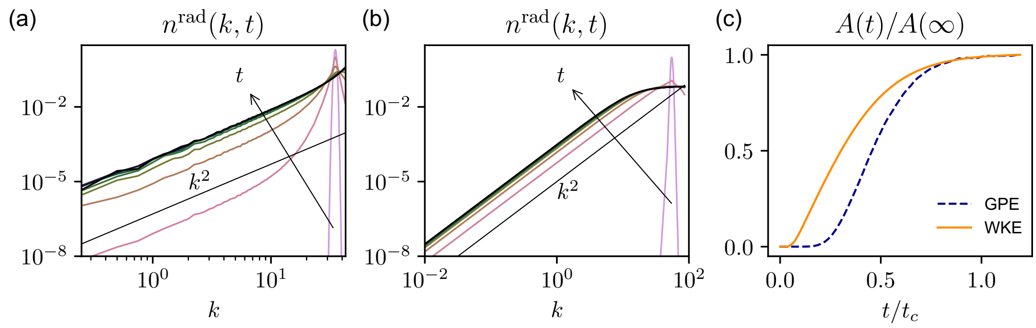

FIG. 5. Numerical results with large E/N: (a) spectrum $n^{\rm rad}(k,t)$ in GPE simulation (case 5) for times $t = 0, 40, 80, 120, ..., 320$; (b) spectrum $n^{\rm rad}(k,t)$ in the WKE simulation (case 2) for times $t = 0, 250, 500, 750, ..., 2000$; (c) values of $A(t)/A(\infty)$ for the prefactor $A(t)$ in the fit $n^{\rm rad}(k,t) = A(t)k^2$ for both cases.

in what follows f_0 is a positive constant. Naturally, $k_{\rm f}$ is taken small for the direct cascade and large for the inverse one. The dissipation term is of the form $D_{\mathbf{k}} = (k/k_{\rm L})^{-2\alpha} + (k/k_{\rm R})^{2\beta}$; it acts at small and/or large scales. Moreover, the condensate mode $k = 0$ is also dissipated with constant friction $D_{\mathbf{0}}$ when necessary. The WKE is forced by adding to its RHS a constant-in-time function $f_\omega = c_{\rm f}\,\Gamma(\omega)$, where $\Gamma(\omega)$ is the Gaussian centered at $\omega_{\rm f}$ and of width $\Delta\omega_{\rm f}$. Dissipation is introduced by adding the term $-[(\omega/\omega_{\rm L})^{-\alpha} + (\omega/\omega_{\rm R})^{\beta}]n_\omega$ to the RHS of the WKE. We perform two WKE simulations—one for the direct cascade and another for the inverse one (cases 9 and 10 in Table II, respectively). All the numerical parameters are given in Table II.

1. Forcing at low k′s: Direct cascade

To implement the direct cascade, we simulate the GPE and the WKE with forcing terms centered at low wave numbers and let the spectrum propagate to large wave numbers (we set no dissipation at large k's). Figures 6 and 7 present numerical results of the GPE and the WKE simulations, respectively (cases 6 and 9 in Table II). Observing the time evolution of the wave-action spectrum in Fig. 7(a), one can see the formation of the log-corrected KZ spectrum behind the front. Thanks to the good scale separation, for this simulation we can also see the quasisteady state behind the wave number where the forcing is imposed. However, the inverse-cascade range is too short and the KZ power law $\sim k^{-1/3}$ is not observed in this case. In Fig. 6(a) for the GPE simulation we also see a curve qualitatively consistent with the log-corrected KZ spectrum which develops behind the front, but the agreement is poorer than for the WKE simulation. The inset in Fig. 6(a) shows the GPE energy $H(t)$ which is increasing nearly linear for all the times, whereas the inset in Fig. 7(a) shows an increase of the WKE energy $E(t)$ which is almost linear for $t > 5$. This dependence $E(t) \sim t$ implies that in the self-similar solution of the first-kind (13) $\lambda = 1$. Using the last equality that gives $b = 1/2$, we plotted the self-similar solutions in Fig. 6(b) for $t \in [100, 160]$ and in Fig. 7(b) for $t \in [2, 17.3]$. In these time intervals, an evident visual collapse of plots can be observed for both GPE and WKE simulations. The time windows, in which we observe clear self-similar evolution, also agree with time windows in which the compensated wavefront $k_{\rm cf}$ is constant (see the insets). Note that in the GPE simulations, we start to lose self-similarity around $t = 180$, because the front touches the right boundary (maximum wave number).

It is worth mentioning that the numerical setup that we used for the direct cascade, mimics the configuration in the experiment by Navon *et al.* [11], with a constant rate of energy injection and almost steady total number of particles. In their study, they reported $b \approx 0.54$ with a tolerance of 6% when converted to our notations. This finding is remarkably close to our theoretical prediction $b = 1/2$.

2. Forcing at high k′s: Inverse cascade

We perform two GPE simulations with the same forcing centered at high k's and hyper-viscosity acting at even higher k's located to the right from the forcing range to achieve the inverse cascade (cases 7 and 8 in Table II). The only difference is that for case 8 we put hypoviscosity at low k's to absorb the inverse cascade of particles and to get a steady state, whereas in case 7 no dissipation at low k's was imposed. Therefore, the two simulations show almost the same behavior before the

TABLE II. Parameters of simulations of forced-dissipated GPE and WKE.

Case	Model	Cascade	L	N_p	$n_{\rm f}$	f_0^2	$k_{\rm f}$	$D_{\mathbf{0}}$	k_L	α	k_R	β
6	GPE	direct	4π	512	1.5	—	1	10^3	—	—	—	—
7	GPE	inverse	2π	512	—	10^{-4}	125	—	—	—	130	6
8	GPE	inverse	2π	512	—	10^{-4}	125	10^3	1	0.5	130	6
Case	Model	Cascade	$\omega_{\rm min}$	$\omega_{\rm max}$	$c_{\rm f}$	$\omega_{\rm f}$	$\Delta\omega_{\rm f}$	$\omega_{\rm L}$	α	$\omega_{\rm R}$	β	$k_{\rm f}$
9	WKE	direct	10^{-5}	10	10	3×10^{-4}	3×10^{-4}	10^{-4}	4	—	—	0.025
10	WKE	inverse	0.1	10^5	50	125^2	500	10	4	$10^5/4.5$	7	—

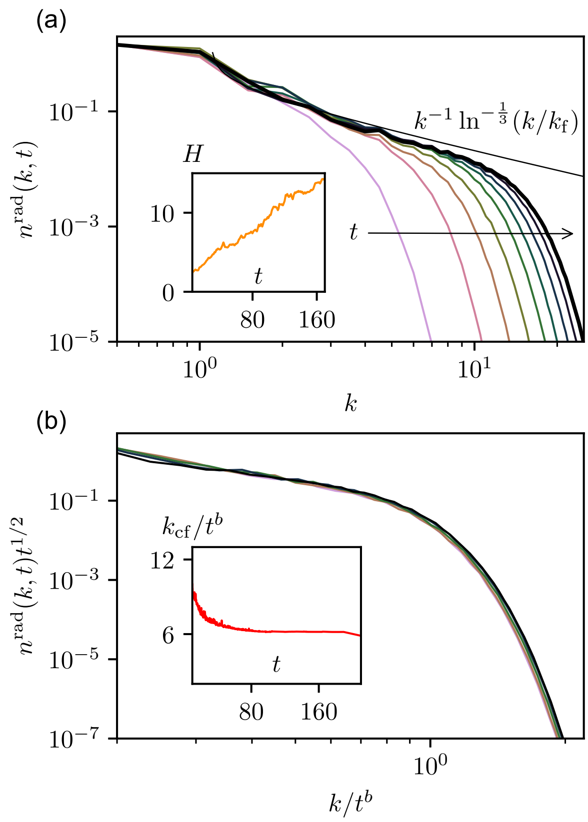

FIG. 6. Numerical results for GPE simulation (case 6) with forcing at low k's. (a) Values of the spectrum $n^{\mathrm{rad}}(k,t)$ for $t = 20, 50, 80, 110, 140, 170, 200, 230, 260$, and in the inset—time evolution of energy density $H(t)$; (b) $n^{\mathrm{rad}}(k,t)$ compensated by $t^{1/2}$ vs compensated wave number k/t^b for $t = 80, 100, 120, 140, 160$ and in the inset—time evolution of the wave front k_{cf} divided by t^b.

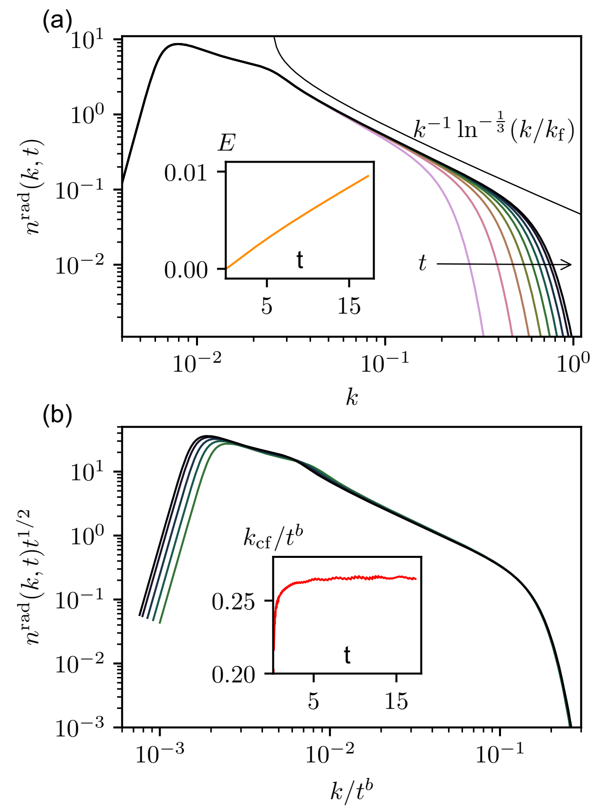

FIG. 7. Numerical results for WKE simulation (case 9) with forcing at low k's. (a) Values of the spectrum $n^{\mathrm{rad}}(k,t)$ for the times $t = 2, 4, 6, 8, 10, 12, 14, 16, 17.3$ and in the inset—time evolution of energy density E; (b) $n^{\mathrm{rad}}(k,t)$ compensated by $t^{1/2}$ vs compensated wave number k/t^b for the times $t = 10, 12, 14, 16, 17.3$ and the inset for the time evolution of wave front k_{cf} divided by t^b.

left parts of the spectral fronts get into the region where the dissipation of case 8 is imposed. Figure 8(a) presents the early time evolution of the wave-action spectra for $t \in [0.85, 1.3]$ obtained for case 7. As in the free-decay simulations, we see a particle equipartition scaling k^2 in the left front and an anomalous k^{-x^*}-scaling with $x^* \approx 0.5$ behind the front. The late time evolution of case 7 is plotted in Fig. 8(b), where we see the $k^{-2.5}$ scaling for small k's and the energy equipartition for large k's, as it was reported in Ref. [28]. It is also similar to the late-time evolution of freely decaying inverse cascade plotted in Fig. 4(a). The final state appears to be quasisteady with condensate ratio $[n^{\mathrm{rad}}(0,t)/N]$ oscillating around 10^{-3}—a picture previously observed in Ref. [28]. Obviously, for the final state to be steady the particle and energy inputs and sinks in the high-k region must cancel each other.

Let us now consider the long-time evolution in case 8. We expect that due to the presence of the dissipation at low k's the system will eventually relax to the steady KZ spectrum corresponding to the inverse cascade of particles, $n_k^{\mathrm{rad}} \sim k^{-1/3}$. The route to this final steady KZ spectrum is interesting; it can be seen in the sequence of spectra plotted in Fig. 8(c) for different moments of the late evolution. Shortly after the anomalous spectrum $\sim k^{-x^*} \approx k^{-0.5}$ forms at $t \to t^* \approx 1.5$, we see a spectrum overshoot at low k's before it relaxes to smaller values after the low-k dissipation takes effect. This is followed by an opposite overshoot characterized by the spectrum depletion and formation of a slope shallower than $k^{-1/3}$. Only after that the spectral slope moves up toward and stabilizes at $-1/3$. This oscillatory relaxation to the KZ steady state is rather different from the reflected wave scenario (corresponding to the self-similarity of the third kind) described at the end of Sec. III.

For the WKE, long-time inverse-cascade evolution exists only if a low-k dissipation is present because otherwise the spectrum blows up at $t = t^*$. Numerical results for this case (case 10 in Table II) are presented in Fig. 9 with spectra shown in panel (a) and the spectral slopes (log-derivatives of n_k^{rad})—in panel (b). Here, we see that the transition from the slope of anomalous exponent $-x^*$ (≈ -0.5) to the KZ slope $-1/3$ proceeds monotonously—faster at lower and slower at higher k's. This is consistent with the reflected wave scenario described at the end of Sec. III. However, the range of wave numbers achievable in numerics is insufficient for making any conclusions about the realizability of third-kind self-similarity.

V. SUMMARY AND DISCUSSION

In this paper, we studied evolving BEC wave turbulence using numerical simulations of the GPE and the WKE in

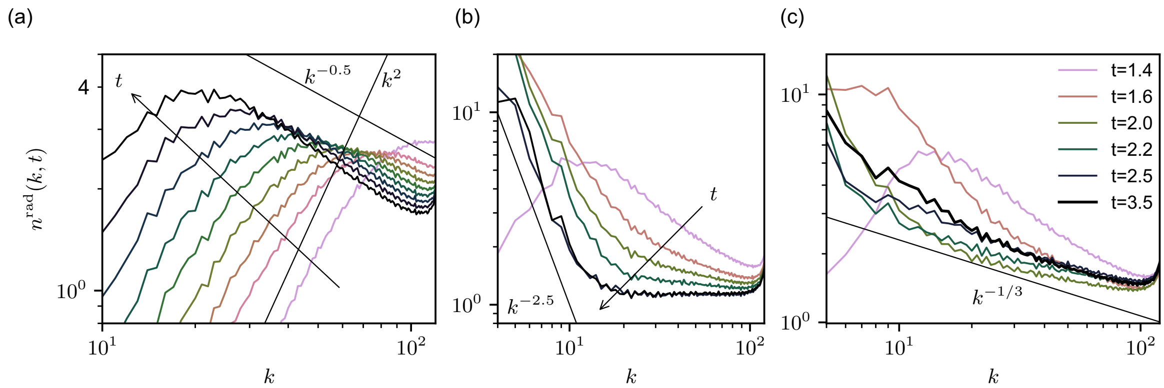

FIG. 8. Numerical results for GPE simulations with forcing at high k's: (a) spectrum $n^{\mathrm{rad}}(k,t)$ (of case 7) for early times $t = 0.85, 0.95, 1, 1.05, 1.1, 1.15, 1.2, 1.25, 1.3$; (b) long-time evolution of $n^{\mathrm{rad}}(k,t)$ (of case 7) without dissipation at low k for times $t = 1.4, 1.6, 1.7, 1.8, 2.4, 3$; (c) long-time evolution of $n^{\mathrm{rad}}(k,t)$ (of case 8) with dissipation at low k's.

several different setups corresponding to free-decaying and forced-dissipated cases for developing inverse, direct and dual cascades. Our focus was on identifying self-similar evolution regimes. In both the GPE and the WKE simulations, we observe the first-kind self-similarity for the direct cascade. In the free-decay simulations, the self-similar spectra tend to stationary thermal energy equipartition states at large times, $t \to \infty$. The temperature of such final states is determined by the total initial energy in the system. For the forced-dissipated setup, the final steady state is the direct-cascade KZ spectrum (which forms immediately behind the propagating front of the self-similar spectrum.

For the inverse cascade evolution, we have verified the existence of the self-similar regime of the second kind describing self-accelerating dynamics of the spectrum leading to blowup at $k = 0$ at a finite time $t = t^*$. Due to the fact that close to t^* the nonlinear dynamics is faster than the forcing process, the self-similar evolution of the second kind is insensitive to the presence or absence of forcing. Physically, this process describes a nonequilibrium Bose-Einstein condensation or, to be more precise, precondensation—because at $t = t^*$ the particle occupation of $k = 0$ is still zero (i.e., the integral of total number of particles (5a) converges at $k = 0$ on the spectrum k^{-x^*}). For WKE, the blowup is exact, meaning that no free-decay evolution can be considered for $t > t^*$ without regularising the WKE model, e.g. via introducing an evolution equation for the $k = 0$ mode and coupling it to the equation for modes with $k > 0$ as was done in Refs. [15,25]. We have not attempted to consider such post-t^* evolution with this kind of regularization. Interestingly, a significant numerical resolution available for the WKE simulations allowed us to implement a dual cascade free-decay system where both the direct cascade (first-kind self-similarity) and the inverse cascade (the second-kind self-similarity) are observed simultaneously for times up to t^*. For GPE, the blowup behavior is only an approximate intermediate asymptotic. Closer to t^* the self-similar behavior breaks down both due to the breakdown of the weak nonlinearity assumption and due to the discreteness of the k-space corresponding to a finite retaining box. As a result, the GPE evolution continues regularly past t^*. Namely, in the absence of low-k dissipation, it shows the formation of an energy equipartition spectrum at high k's and a sharp spectrum in the low-k region—a condensate. We emphasize the fact that in the case of the GPE system in a finite (periodic) box, the condensate is spread over few lowest-k modes and not concentrated at $k = 0$ only as in the WKE case. In the presence of low-k dissipation, in both the WKE and the GPE systems,

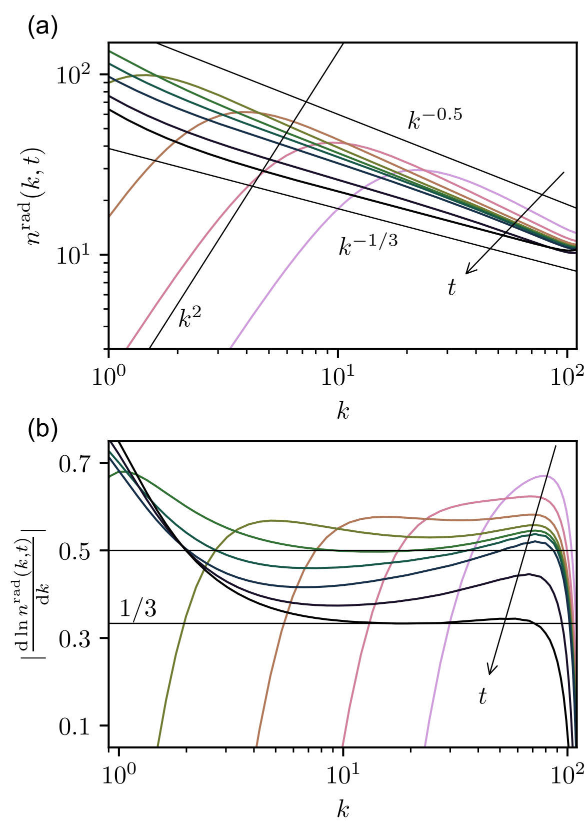

FIG. 9. Numerical results obtained by WKE simulation (case 10) with forcing at intermediate k's and dissipation at both low and high k's: (a) spectrum $n^{\mathrm{rad}}(k,t)$ for times $t = 0.0176$, $0.0185, 0.0190, 0.0192, 0.0194, 0.0195, 0.0197, 0.0210, 0.0379$; (b) slope of $\ln n^{\mathrm{rad}}(k)$ for the same times as in panel (a).

the condensate is suppressed and the spectrum relaxes to the KZ inverse cascade steady state. For the GPE, an oscillation is observed in the transient period, whereas for the WKE system (which is now regularized by the low-k dissipation and can evolve for $t > t^*$) we see signatures of the reflected wave scenario characterized by the third-type self-similarity. However, these signatures are quite indirect and more work is needed for identifying the third-type self-similarity which, in our case, still remains hypothetical. Besides numerical simulations for a much wider range of k, which would presently be hard to achieve, one could solve directly the integro-differential equation for the self-similar shape in a way similar to the one used for a three-wave kinetic equation for MHD waves in Ref. [23]. This could be an interesting problem for future study.

Finding universal dynamics in turbulent superfluid Bose gases has gained significant interest in recent laboratory experiments (see Refs. [11,46–48]). These experiments involve the self-similar regimes discussed in the paper. In particular, the experiments detailed in Refs. [11,46] have reported instances of the first kind of self-similarities for the direct cascade. These cases encompass scenarios involving free-decay with nearly constant energy and forced cases with linearly increasing energy, respectively. Remarkably, the exponent constants observed in these experiments closely align with our predictions by Eq. (13) for both configurations. However, the experimental investigation of the inverse cascade poses a more intricate challenge than the direct cascade. Recent experiments conducted in Refs. [46–48] aimed to detect self-similarity of the first kind. It is important to note that, as clarified in the current paper, in the inverse cascade, the second kind of self-similarity should be expected instead, and therefore, the respective experiments should be revised and refined.

Finally, special interest for future studies presents 2D setups relevant to optical turbulence systems, see, e.g., Ref. [39]. Note that 2D systems are special and different from 3D ones since neither true condensation nor pure KZ cascades are possible for such systems. Also, since the 2D optical systems are usually trapped by a carrier beam, the system may remain weakly nonlinear even if a significant part of the total particles accumulate in the ground energy state, as it was the case in experiment of Ref. [39]. Evolving 2D BEC WT is also very different from the 3D evolving turbulence, requiring a separate theoretical investigation.

ACKNOWLEDGMENTS

This work was funded by the Simons Foundation Collaboration grant Wave Turbulence (Award ID No. 651471). This work was granted access to the high-performance computing facilities under GENCI (Grand Equipement National de Calcul Intensif) Grant No. A0102A12494 (IDRIS and CINES), the OPAL infrastructure from Université Côte d'Azur, supported by the French government, through the UCAJEDI Investments in the Future project managed by the National Research Agency (ANR) under Reference No. ANR-15-IDEX-01. The work of Boris Semisalov was supported by the RSF (Agreement No. 22-11-00287).

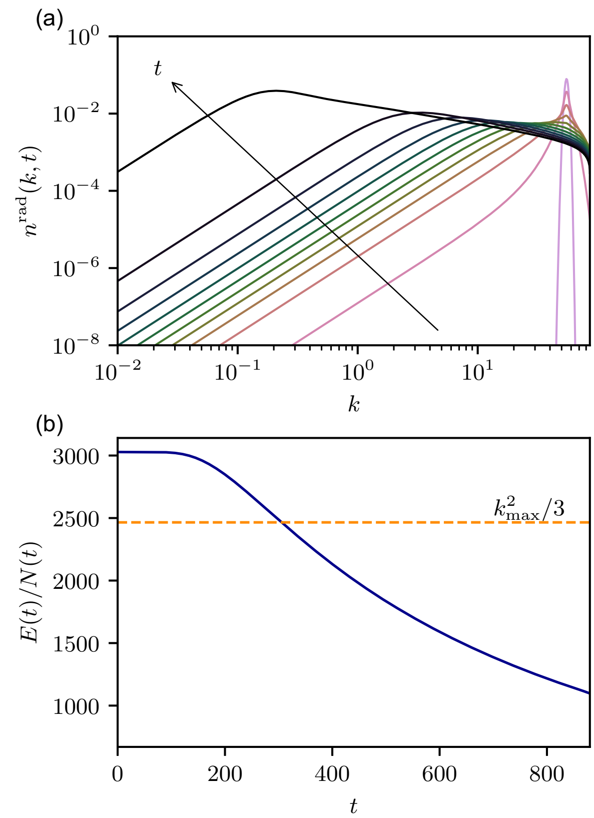

FIG. 10. Numerical results for WKE with the leak of energy: (a) spectrum $n^{\mathrm{rad}}(k,t)$ for times $t = 0, 80, 160, 240, ..., 880$; (b) relation E/N depending on time.

APPENDIX: NAIVE TRUNCATION OF THE WAVE KINETIC EQUATION

As discussed in Sec. III D 2, a proper truncation is needed to conserve the invariants. In this Appendix, we show the spurious consequences of the naive truncation. Namely, we impose the cutoff $\omega_{\max}$ in the collision term, but keep the subdomains Ω_2, Δ_1, and Δ_2 sketched in Fig. 1.

We repeat the simulation of case 2 in Table I using this truncation scheme. Despite the facts that for such conditions $E/N \approx 3028 > k^2_{\max}/3 \approx 2465$ and the initial spectrum does not touch $\omega_{\max}$, we got blowup in a finite time, see Fig. 10(a).

The reason for this effect can be extracted from Fig. 10(b). The relation E/N starts to decrease rapidly at $t \sim 150$, and for $t = 300$ we already have $E/N < k^2_{\max}/3$. Let t_c be the time when the equality $E/N = k^2_{\max}/3$ is reached. In Fig. 10(a) one can see that for $t < t_c$ the evolution of spectrum slows down and RJ spectrum starts to develop, but for $t > t_c$ the evolution accelerates and spectrum goes to blowup. The reason is that the condition $E/N < k^2_{\max}/3$ is dynamically broken as a consequence of the energy leak.

This spurious evolution is an effect of the naive UV-cutoff only and, by using finer frequency and time discretizations, we have verified that it is not caused by finite grid effects or time stepping.

[1] V. Zakharov, V. L'vov, and G. Falkovich, *Kolmogorov Spectra of Turbulence I, Wave Turbulence*, Springer Series in Nonlinear Dynamics (Springer, Berlin, 1992).
[2] S. Nazarenko, *Wave Turbulence*, Vol. 825 (Springer Science & Business Media, Cham, 2011).
[3] S. Galtier, Frontmatter, in *Physics of Wave Turbulence* (Cambridge University Press, Cambridge, UK, 2022), pp. i–iv.
[4] V. E. Zakharov and N. N. Filonenko, J. Appl. Mech. Tech. Phys. **8**, 37 (1967).
[5] P. Caillol and V. Zeitlin, Dyn. Atmos. Oceans **32**, 81 (2000).
[6] S. Galtier, Phys. Rev. E **68**, 015301(R) (2003).
[7] S. Dyachenko, A. Newell, A. Pushkarev, and V. Zakharov, Physica D **57**, 96 (1992).
[8] V. S. L'vov and S. Nazarenko, Low Temp. Phys. **36**, 785 (2010).
[9] D. Proment, S. Nazarenko, and M. Onorato, Physica D **241**, 304 (2012).
[10] S. Galtier and S. V. Nazarenko, Phys. Rev. Lett. **119**, 221101 (2017).
[11] N. Navon, C. Eigen, J. Zhang, R. Lopes, A. L. Gaunt, K. Fujimoto, M. Tsubota, R. P. Smith, and Z. Hadzibabic, Science **366**, 382 (2019).
[12] S. Nazarenko and S. Lukaschuk, Annu. Rev. Condens. Matter Phys. **7**, 61 (2016).
[13] A. Griffin, G. Krstulovic, V. S. L'vov, and S. Nazarenko, Phys. Rev. Lett. **128**, 224501 (2022).
[14] Y. Zhu, B. Semisalov, G. Krstulovic, and S. Nazarenko, Phys. Rev. Lett. **130**, 133001 (2023).
[15] D. V. Semikoz and I. I. Tkachev, Phys. Rev. Lett. **74**, 3093 (1995).
[16] L. Pítajevskíj and S. Stringari, *Bose–Einstein Condensation*, International Series of Monographs on Physics (Clarendon Press, Oxford, UK, 2003).
[17] V. Zakharov, S. Musher, and A. Rubenchik, Phys. Rep. **129**, 285 (1985).
[18] D. Proment, S. Nazarenko, and M. Onorato, Phys. Rev. A **80**, 051603(R) (2009).
[19] N. Navon, A. L. Gaunt, R. P. Smith, and Z. Hadzibabic, Nature (London) **539**, 72 (2016).
[20] C. Connaughton, C. Josserand, A. Picozzi, Y. Pomeau, and S. Rica, Phys. Rev. Lett. **95**, 263901 (2005).
[21] G. Krstulovic and M. Brachet, Phys. Rev. Lett. **106**, 115303 (2011).
[22] G. Krstulovic and M. Brachet, Phys. Rev. E **83**, 066311 (2011).
[23] N. K. Bell and S. V. Nazarenko, J. Phys. A: Math. Theor. **51**, 405501 (2018).
[24] S. Nazarenko, V. Grebenev, S. Medvedev, and S. Galtier, J. Phys. A: Math. Theor. **52**, 155501 (2019).
[25] D. V. Semikoz and I. I. Tkachev, Phys. Rev. D **55**, 489 (1997).
[26] B. Semisalov, V. Grebenev, S. Medvedev, and S. Nazarenko, Commun. Nonlin. Sci. Numer. Simul. **102**, 105903 (2021).
[27] R. Lacaze, P. Lallemand, Y. Pomeau, and S. Rica, Physica D **152-153**, 779 (2001).
[28] V. Shukla and S. Nazarenko, Phys. Rev. A **105**, 033305 (2022).
[29] Y. Zhu, B. Semisalov, G. Krstulovic, and S. Nazarenko, Phys. Rev. E **106**, 014205 (2022).
[30] N. G. Berloff and B. V. Svistunov, Phys. Rev. A **66**, 013603 (2002).
[31] G. Düring, A. Picozzi, and S. Rica, Physica D **238**, 1524 (2009).
[32] M. Escobedo and J. Velázquez, *On the Theory of Weak Turbulence for the Nonlinear Schrodinger Equation*, Memoirs of the American Mathematical Society (American Mathematical Society, Providence, RI, 2015).
[33] T. D. Lee, Q. Appl. Math. **10**, 69 (1952).
[34] R. H. Kraichnan, Phys. Fluids **10**, 1417 (1967).
[35] C. Cichowlas, P. Bonaïti, F. Debbasch, and M. Brachet, Phys. Rev. Lett. **95**, 264502 (2005).
[36] G. Krstulovic, P. D. Mininni, M. E. Brachet, and A. Pouquet, Phys. Rev. E **79**, 056304 (2009).
[37] S. S. Ray, U. Frisch, S. Nazarenko, and T. Matsumoto, Phys. Rev. E **84**, 016301 (2011).
[38] G. Krstulovic, M.-E. Brachet, and A. Pouquet, Phys. Rev. E **84**, 016410 (2011).
[39] K. Baudin, A. Fusaro, K. Krupa, J. Garnier, S. Rica, G. Millot, and A. Picozzi, Phys. Rev. Lett. **125**, 244101 (2020).
[40] M. J. Davis, S. A. Morgan, and K. Burnett, Phys. Rev. Lett. **87**, 160402 (2001).
[41] G. Krstulovic and M. Brachet, Phys. Rev. B **83**, 132506 (2011).
[42] U. Giuriato and G. Krstulovic, Phys. Rev. B **103**, 024509 (2021).
[43] V. Shukla, P. D. Mininni, G. Krstulovic, P. C. di Leoni, and M. E. Brachet, Phys. Rev. A **99**, 043605 (2019).
[44] G. Krstulovic, A theoretical description of vortex dynamics in superfluids. Kelvin waves, reconnections and particle-vortex interaction, Habilitation à diriger des recherches, Universite Côte d'Azur, 2020, https://hal.science/tel-03544830v1.
[45] B. V. Semisalov, Numer. Anal. Appl. **15**, 63 (2022).
[46] J. A. Glidden, C. Eigen, L. H. Dogra, T. A. Hilker, R. P. Smith, and Z. Hadzibabic, Nat. Phys. **17**, 457 (2021).
[47] A. D. García-Orozco, L. Madeira, M. A. Moreno-Armijos, A. R. Fritsch, P. E. S. Tavares, P. C. M. Castilho, A. Cidrim, G. Roati, and V. S. Bagnato, Phys. Rev. A **106**, 023314 (2022).
[48] L. Madeira, A. García-Orozco, M. Moreno-Armijos, A. Fritsch, and V. Bagnato, arXiv:2308.15646.